Visualisation of floatation of tunnels following earthquake induced liquefaction

By

Emily Room (St John's)

Fourth year undergraduate project

In Group D, 2013/2014

I hereby declare that, except where specifically indicated, the work submitted herein is my own original work.

EMILY Room ERoom 28/05/14

Technical abstract

The purpose of this project was to observe and record the floatation mechanisms of rectangular tunnels and to compare these results with the results of previous work done on the floatation mechanisms of circular tunnels and identify differences between these mechanisms. Rectangular tunnels were chosen for study because, although the vast majority of tunnels and pipelines and other key features of underground infrastructure are circular, many vital areas of infrastructure such as road and rail tunnels are rectangular. As such, it is important that any differences between rectangular and circular tunnel floatation mechanisms are identified.

Three experiments were carried out on the Schofield Centre's 1g shaking table, using a model tunnel of dimensions 300 x 200 x 80mm and constructed from ¼" thick aluminium plate. This model was buried in loose Hostun sand which was fully saturated with water at burial depths of 50mm, 100mm and 200mm. These burial depths corresponded with a factor of safety against floatation of 1.07, 1.63 and 2.74 respectively. The model was then shaken by a vibration with a frequency of 5Hz and amplitude of 5mm for a duration of 10 seconds. The vertical acceleration, horizontal acceleration and uplift displacement of the tunnel were all recorded, as was the ground displacement and pore pressure in the soil immediately below the tunnel and away from the tunnel. The experiment was recorded using a high speed camera at 44 frames per second.

The conclusions which were drawn from this project were that increased burial depth reduces the degree of liquefaction which occurs, the uplift displacement of a tunnel during floatation decreases with increased burial depth and the flow of soil around a rectangular tunnel is superficially similar to the flow of fluid around a rectangular cylinder and as such is more turbulent than the flow of soil around a circular tunnel during floatation, causing rotation of the tunnel and the formation of voids beneath it.

1 - Introduction

Liquefaction of soil is a phenomenon which occurs during earthquakes, causing severe destruction of buildings and infrastructure. During liquefaction, pore pressures in the soil increase, the soil loses strength and stiffness and the soil begins to behave like a thick liquid. As the soil loses a significant proportion of its strength and stiffness, it becomes no longer able to support structures and so foundations fail, surface structures collapse and sink, and buried lightweight structures float towards the ground surface.

Liquefaction has been a major cause of destruction in several well-documented earthquakes including the 1964 Niigata earthquake in Japan, the 1989 Loma Prieta earthquake in San Francisco and the recent 2010 and 2011 earthquakes in Canterbury and Christchurch in New Zealand. Figures 1.1 and 1.2 below show examples of the damage caused by tunnel floatation due to soil liquefaction during the 2010 Canterbury earthquake and the 2011 Tohoku earthquake in Japan.

Fig. 1.1 – Uplifted pipeline in Canterbury, NZ

Fig. 1.2 – Uplifted pipeline in Tokyo, Japan

Given the severity and extent of the damage that can be caused by tunnel floatation during earthquake-induced liquefaction, it is important that the floatation mechanisms of tunnels in liquefied soils are understood so that suitable measures can be taken to prevent future damage occurring.

1.1 - Liquefaction

The phenomenon of liquefaction occurs when loosely packed, saturated, sandy or low-plasticity silty soils are sheared rapidly and cyclically, such as by an earthquake. Liquefaction causes significant loss of soil strength and stiffness, reducing the bearing capacity of the soil drastically and often with catastrophic results for structures built on the now liquefied ground.

When loose sand is sheared, it contracts to a more efficient, denser packing arrangement. If this loose sand is dry, then the air in the voids can readily escape from the sand and allow it to contract. If the sand is saturated and the shearing is slow enough, the water in the voids can also readily escape and the sand continues to behave in a drained manner. When saturated sand is sheared rapidly, the water cannot escape at the rate at which the loading occurs and so the pore water pressure increases as the voids try to collapse.

The increase in pore water pressure causes the effective stress to decrease in accordance with Terzaghi's principle of effective stress as stated in Equation 1.1 below, in which σ is total stress, σ' is effective stress and u is pore water pressure.

$$\sigma' = \sigma - u \; (1.1)$$

The effective stress is what gives soil strength and stiffness – under very low effective stress, soil has very little strength or stiffness. Full liquefaction occurs when the effective stress is zero. At this point the sand becomes completely buoyant.

A buried structure will float if the buoyant weight of sand above the structure and the structure's own self weight is less than the buoyancy force acting on the structure due to hydrostatic pressure. As the effective stress decreases and the pore water pressure increases, the buoyant weight of the sand decreases. Once the buoyant weight of the sand is low enough, the buried structure will float.

1.2 - Project aims

The purpose of this project is to observe and record the floatation mechanisms of rectangular tunnels and to compare these results with the results of previous work done on the floatation mechanisms of circular tunnels and identify differences between these mechanisms. The reason for looking at rectangular tunnels is that, although the vast majority of tunnels and pipelines and other key features of underground infrastructure are circular, many vital areas of infrastructure such as road and rail tunnels are rectangular. As such, it is important that any differences between rectangular and circular tunnel floatation mechanisms are identified.

1.3 - Expected results

The results of previous work conducted on the floatation mechanism of circular tunnels showed that soil flows around a circular tunnel during floatation in a manner which is superficially similar to the flow of a viscous fluid around a cylinder, with the quiver plots generated by particle image velocimetry (PIV) analysis of the soil motion resembling the streamlines around a cylinder in a viscous flow. As such, it is expected that the flow of soil around a rectangular tunnel during floatation will be similar to the flow of a viscous fluid around a cuboid. Figure 1.3 shows the fluid flow around a rectangular cylinder, which should be similar to the soil movements recorded during the experiments.

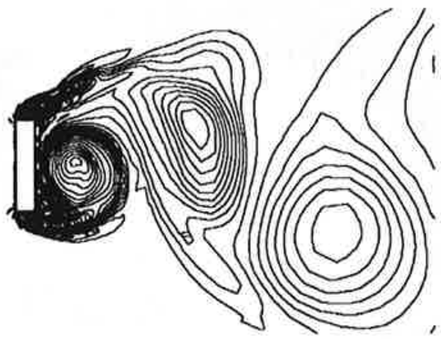

Figure 1.3 – Fluid flow around a rectangular cylinder (Matsukawa and Nakamura, 1987)

It is also expected that increasing the burial depth will decrease the uplift displacement of the buried tunnel during floatation.

2 - Literature review

2.1 – Floatation of Underground Structures in Liquefiable Soils, (Chian, 2012)

Work has already been carried out by Chian (2012) which details the floatation mechanism of circular tunnels. These experiments consisted of a series of dynamic centrifuge tests examining the floatation of circular tunnels of varying diameters and burial depths in saturated sand. The tests were recorded using a high speed camera and PIV analysis of the resulting images was conducted. Figure 2.1.1 shows the typical results of PIV analysis of the soil flow around a circular tunnel.

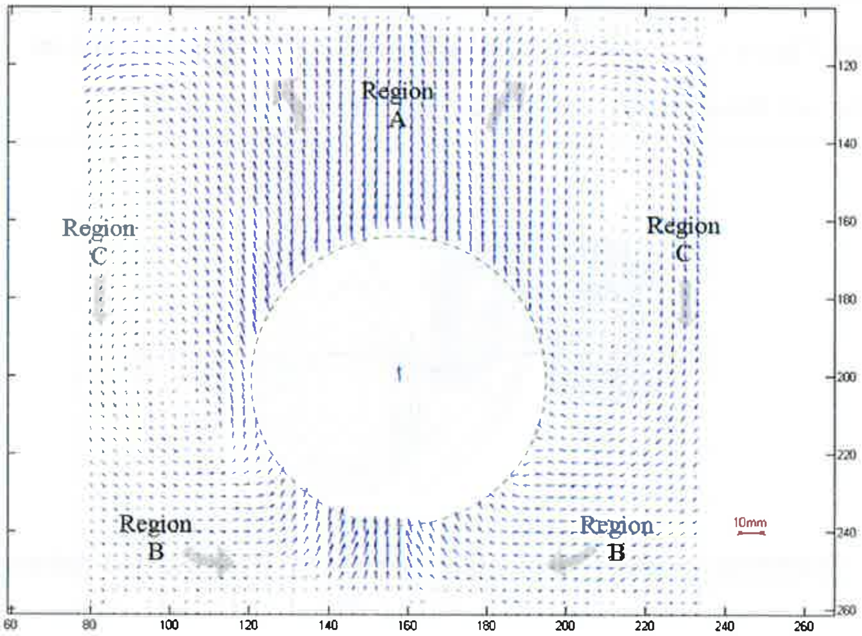

Figure 2.1.1 – Typical results of PIV analysis from Chian (2012)

As stated above, this quiver plot closely resembles the streamlines around a cylinder in viscous flow.

It was also found that increasing the burial depth to diameter ratio of the tunnel resulted in a smaller uplift displacement.

2.2 – Liquefaction and flow failure during earthquakes (Ishihara, 1993)

This lecture summarises the main findings related to liquefaction at the time, discussing the mechanisms of liquefaction, the types of failure that can occur during liquefaction and the conditions required for liquefaction to occur.

Liquefaction is described as a phenomenon in which loose deposits of sand undergo sudden changes into flows much like those of a viscous fluid, and one which frequently occurs during earthquakes if the soil consists of loose, saturated, sandy deposits.

Looseness of the soil and whether or not the soil is sandy are identified as the key factors determining whether or not a soil deposit will liquefy. It is noted that plastic silty soils and clayey soils will not undergo liquefaction, nor will soils which are dense enough to have an SPT blow count greater than around 30.

3 - Apparatus and Instrumentation

3.1 - Tunnel model

The tunnel used throughout the experiments was a cuboid measuring 200x300x80mm and constructed from 1/4" thick aluminium. Plates of PTFE were glued to the ends of the tunnel to ensure it remained watertight during the experiments. The total weight of the tunnel was 24.8N – a total mass of 2.5kg. Figure 3.1.1 shows a photograph of the tunnel model, showing the PTFE plates glued to the ends.

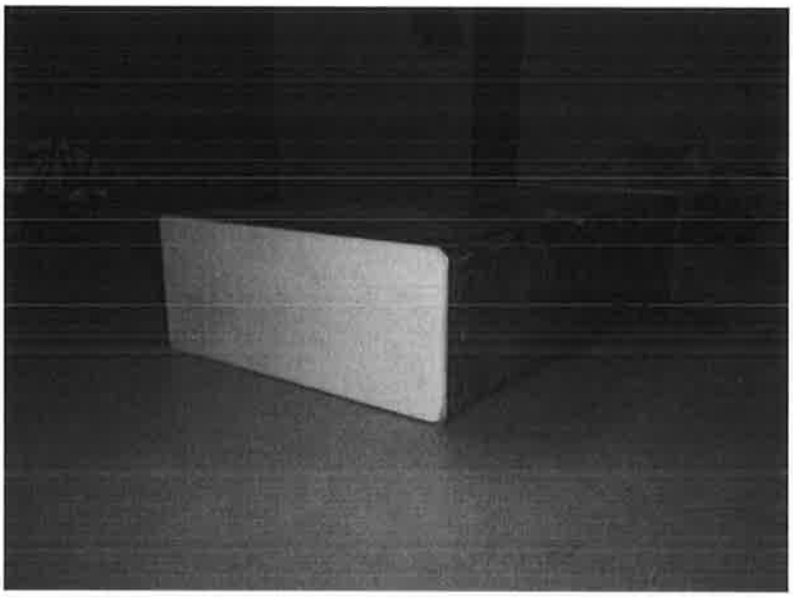

Figure 3.1.1 – Tunnel model

3.2 - Soil model

The sand used during the experiments was Hostun sand – a fine-grained silica sand with a specific gravity of 2.65, a maximum voids ratio of 1.067, a minimum voids ratio of 0.555 and a critical friction angle of 30°. The sand was saturated using water.

3.2.1 - Burial depth

The tunnel was buried at depths of 50, 100 and 200mm, corresponding to burial depth to diameter ratios of 0.25, 0.5 and 1 respectively. The factor of safety against floatation of the tunnel and the required increase in pore pressure to induce floatation was calculated using simple buoyancy calculations as detailed in Appendix A.

Tunnel floatation occurs when the total of the force acting on the tunnel due to the buoyant weight of sand above the tunnel and the self-weight of the tunnel itself is less than the resultant force acting on the tunnel due to the hydrostatic pressure difference between the top and bottom surfaces of the tunnel. Assuming that the pore pressure above and below the tunnel increases by the same amount, the buoyancy force acting on the tunnel will not actually change. However, the increased pore pressure will decrease the buoyant weight of the sand and thus will decrease the force keeping the tunnel buried.

Full liquefaction occurs when the effective stress reaches zero; the pore pressure is equal to the total vertical stress.

The table in Figure 3.2.1 shows the factor of safety against floatation and the required increase in pore pressure for both floatation and full liquefaction. The factor of safety against floatation is calculated as the combined force of the weight of the sand and the self-weight of the tunnel divided by the buoyancy force acting on the tunnel.

Experiment	Burial depth (mm)	FoS against floatation	Required excess pore pressure for floatation (kPa)	Required excess pore pressure for full liquefaction (kPa)
1	50	1.07	0.06	0.435
2	100	1.63	0.49	0.869
3	200	2.74	1.36	1.738

Figure 3.2.1 – Table of factors of safety against floatation and required increases in pore pressure for floatation and full liquefaction

Full details of the calculations used to generate these factors and values are detailed in Appendix A.

3.3 - Shaking table

The cyclic shearing required to induce liquefaction will be induced in the model by setting up the model on the Schofield Centre's 1g shaking table. The shaking table consists of a flywheel coupled to a drive shaft with an offset mass and controlled by a computer to deliver a vibration of a specific frequency and amplitude. In order to ensure that liquefaction takes place, a vibration with a frequency of 5Hz and amplitude of 5mm will be used – the highest amplitude and frequency that the shaking table can produce. This corresponds to a peak ground acceleration of 0.5g. The earthquake duration was 10 seconds.

3.4 - Microelectromechanical (MEM) accelerometers

MEMs accelerometers were attached to the tunnel in order to record the vertical and horizontal acceleration of the tunnel. The rating of the accelerometers used – the maximum acceleration which the accelerometers are capable of measuring – was 1.7g. This is above the maximum expected ground acceleration of 0.5g but still close enough to this value to provide sufficient resolution for the measurements of the tunnel's accelerations.

3.5 - Pore pressure transducers

Pore pressure transducers were placed in the model just below the tunnel and away from the tunnel at the same depth. The transducers will measure the pore pressure during the experiment and so any increase in pore pressure will be recorded which will allow the extent of the liquefaction to be calculated. The pore pressure transducers used during the experiments were rated to 35kPa, making them sensitive enough to provide sufficient resolution in the recorded pore pressure changes.

3.6 - Linear variable differential transformer

A linear variable differential transformer (LVDT) was set up to record the displacement of the shaking table rig during the experiment. This was used to obtain the ground acceleration which can then be compared with the data from the accelerometers attached to the tunnel.

3.7 - Draw wire

A draw wire was attached to the centre of the top surface of the tunnel to record the vertical displacement of the tunnel during floatation.

3.8 - Junction box and datalogging software

The instruments were all connected to a junction box and the signals then passed to a datalogger. The junction box was configured appropriately to the inputs. The datalogging software used for the experiments was DASYLAB 9.0, as used standardly in the Schofield Centre.

4 - Model setup

4.1 - Sand pouring

The sand was poured into the model manually using a hopper. In order for liquefaction to take place, the sand needed to be loosely packed. The conditions required for this to occur when pouring are a high flow rate and a small distance between the end of the nozzle and the surface of the sand. The relative density achieved by this pouring method was approximately 0.4.

To minimise the risk of weak strata of sand forming, the sand layers were poured perpendicularly to each other as shown in Figure 4.1.1 below.

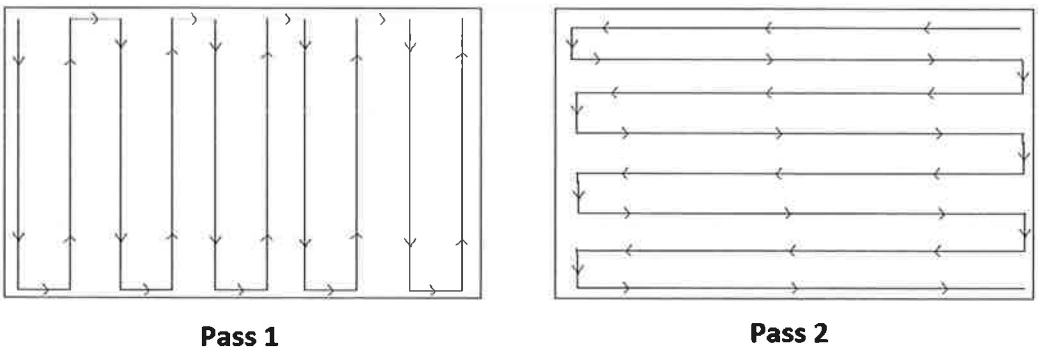

Figure 4.1.1 – Sand pouring technique

To minimise the health and safety risks created by exposure to fine silica sand dust, dust masks with air filters were used during pouring. Full details on the steps taken to mitigate health and safety risks are detailed in Appendix B.

4.2 - Sand dying

The original intention for this set of experiments was to carry out particle image velocimetry (PIV) analysis. With this in mind, around 10% of the sand was dyed blue using metallic ink and then mixed evenly with the undyed sand. This was to create additional texture in the sand and to improve the quality of the PIV analysis by making it easier for the software to track soil patches. The ink was mixed into the sand by hand, and the dyed sand was mixed with the undyed sand by hand in the hopper before pouring. It was thought that the addition of the dye will have no effect on the properties of the sand.

4.3 - Saturation method

The sand was saturated by taping 6mm PVC piping to the bottom of the tank before pouring in the sand. The ends of the PVC piping were sealed so as to be watertight and 1mm diameter holes were punched into the piping along its length at roughly 10mm intervals. This was to ensure that the water flow into the sand was as evenly distributed as possible and slow enough not to cause piping failure of the sand. The holes were then covered with filter paper so as to prevent them becoming clogged with sand during the saturation process. This saturation method was adapted from the one used by Cameron (2013). Figure 4.3.1 below shows the PVC piping in place at the bottom of the shaking table rig before sand pouring begins.

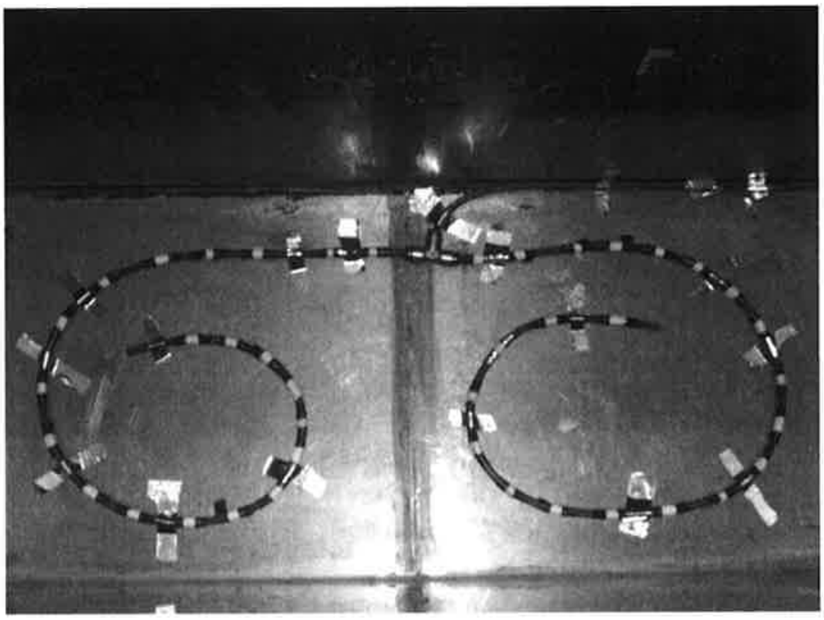

Fig. 4.3.1 – PVC pipes in place before sand pouring

The sand was saturated from the bottom of the tank to ensure that the air in the voids would easily leave the sand and so the sand would be fully rather than partially saturated. Saturation continued until a thin layer of water was present on top of the sand to further ensure full saturation and to ensure that no negative pore pressures were present in the sand. Figure 4.3.2 shows the finished model with the tunnel, instrumentation and sand in place and with the sand fully saturated.

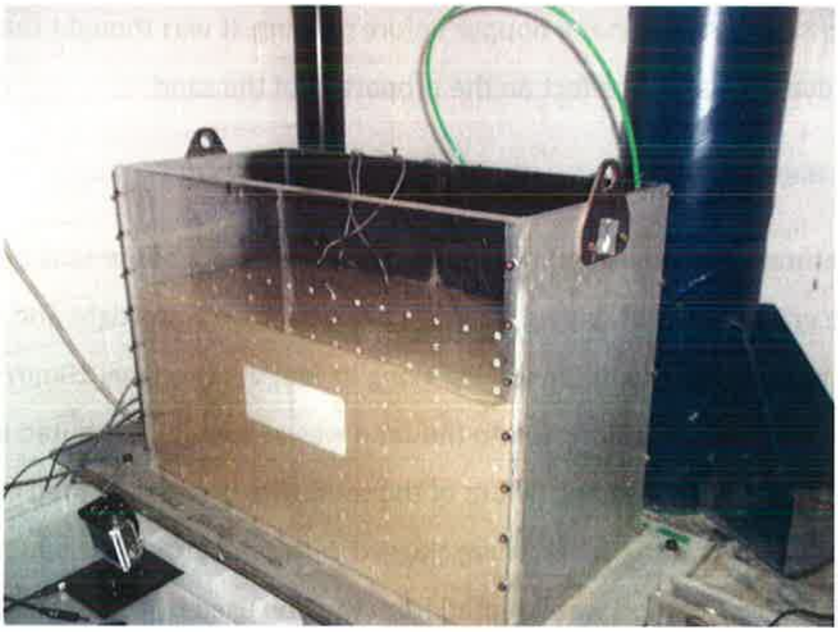

Figure 4.3.2 – Completed model

5 - Floatation of tunnels of different burial depths

5.1 - Test 1 – burial depth: 50mm

5.1.1 - Results

Figure 5.1.1 below shows the graphs of uplift displacement, excess pore pressure generated, vertical acceleration and ground acceleration for the first test, which was carried out at a burial depth of 50mm.

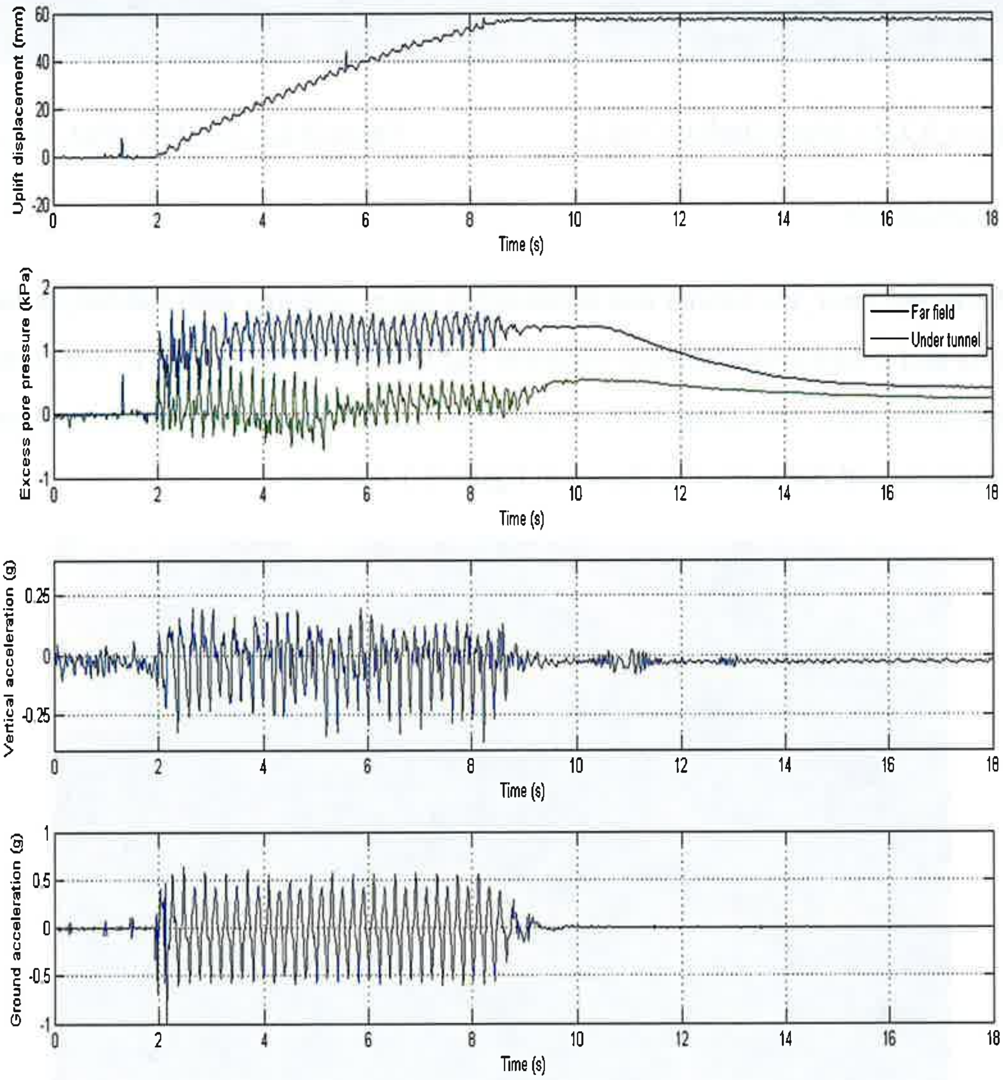

Fig. 5.1.1 – Plots of uplift displacement, excess pore pressure, vertical acceleration and ground acceleration for Test 1

Figures 5.1.2 and 5.1.3 show the model before and after the experiment.

Figure 5.1.2 – Model before Test 1

Figure 5.1.3 – Model after Test 1

5.1.2 – Observations

During the experiment, the tunnel was observed to move upwards with sudden, rather jerky movements and a void formed below the lower right corner of the tunnel as it rotated during the earthquake. Analysing the recorded high speed camera footage by eye shows that the soil flows around the tunnel as shown in Figure 5.1.4 below.

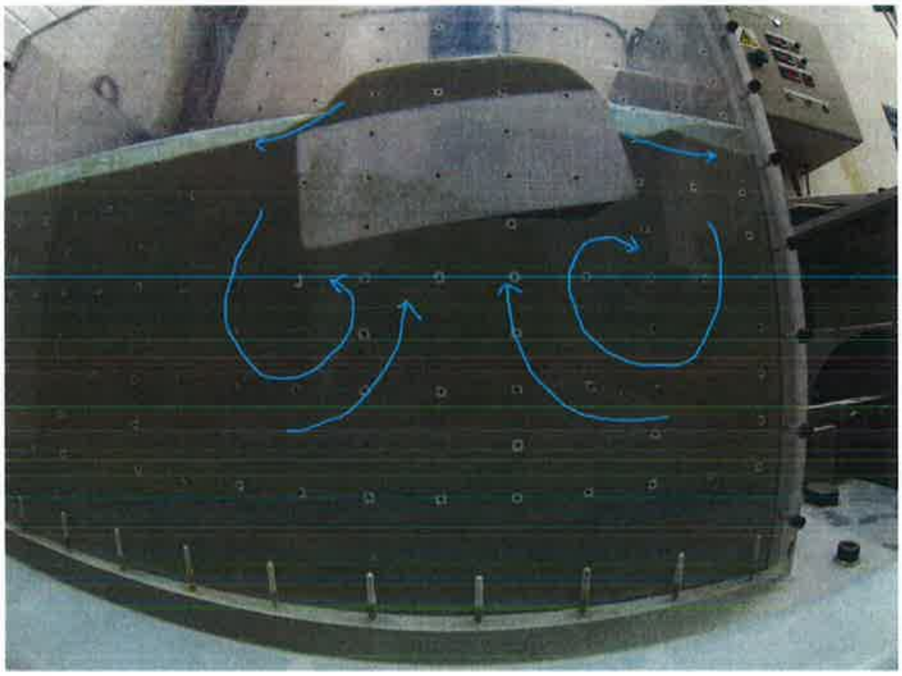

Figure 5.1.4 – Diagram of observed soil movement during Test 1

As can be seen from the image, there was some degree of turbulence and “swirling” of the soil as it moved during the experiment, particularly immediately below the lower corners of the tunnel.

5.1.3 – Excess pore pressures

The second graph in Figure shows that an average excess pore pressure of 1.23kPa is generated in the far-field during the earthquake, with the excess pore pressure after the earthquake before dissipation occurs being 1.356kPa. The average excess pore pressure generated beneath the tunnel during shaking is 0.15kPa with the excess pore pressure present after the shaking has stopped but before dissipation occurs being 0.521kPa. During the shaking, negative pore pressures are generated of up to -0.52kPa.

The calculations outlined in Appendix A suggest that an excess pore pressure of 0.06kPa is sufficient for floatation to occur and that an excess pore pressure of 0.435kPa is sufficient for full liquefaction to occur. The excess pore pressures generated both beneath the tunnel and in the far-field are more than sufficient to cause full liquefaction of the sand, and in fact are high enough to generate negative excess pore pressures. With the excess pore pressures being so far above the value needed for floatation to occur, significant uplift displacements would be expected, as shown by the post-earthquake image in Figure 5.1.3 which shows the tunnel has actually floated above the surface of the sand.

5.1.4 - Vertical acceleration

The peak recorded vertical acceleration is around 0.2g with a peak-to-peak vertical acceleration of 0.4g. The vertical acceleration oscillates at the same frequency as the ground acceleration and the excess pore pressures. The negative vertical accelerations are consistent with both the observed, jerky movement of the tunnel during the earthquake and the oscillation of the pore pressure above and below the value at which floatation occurs.

5.1.5 - Uplift displacement

Based on the excess pore pressure values and the fact that full liquefaction occurs during the experiment, a significant uplift displacement would be expected. This is confirmed by the both the observation made during the experiment and shown in Figure 5.1.3 that the tunnel broke the surface of the sand. The actual recorded uplift was found to be 56.62mm, around 6.5mm greater than the tunnel's original burial depth.

5.2 - Test 2 – burial depth : 100mm

5.2.1 - Results

Figure 5.2.1 below shows the graphs of uplift displacement, excess pore pressure generated, vertical acceleration and ground acceleration for the second test, which was carried out at a burial depth of 100mm.

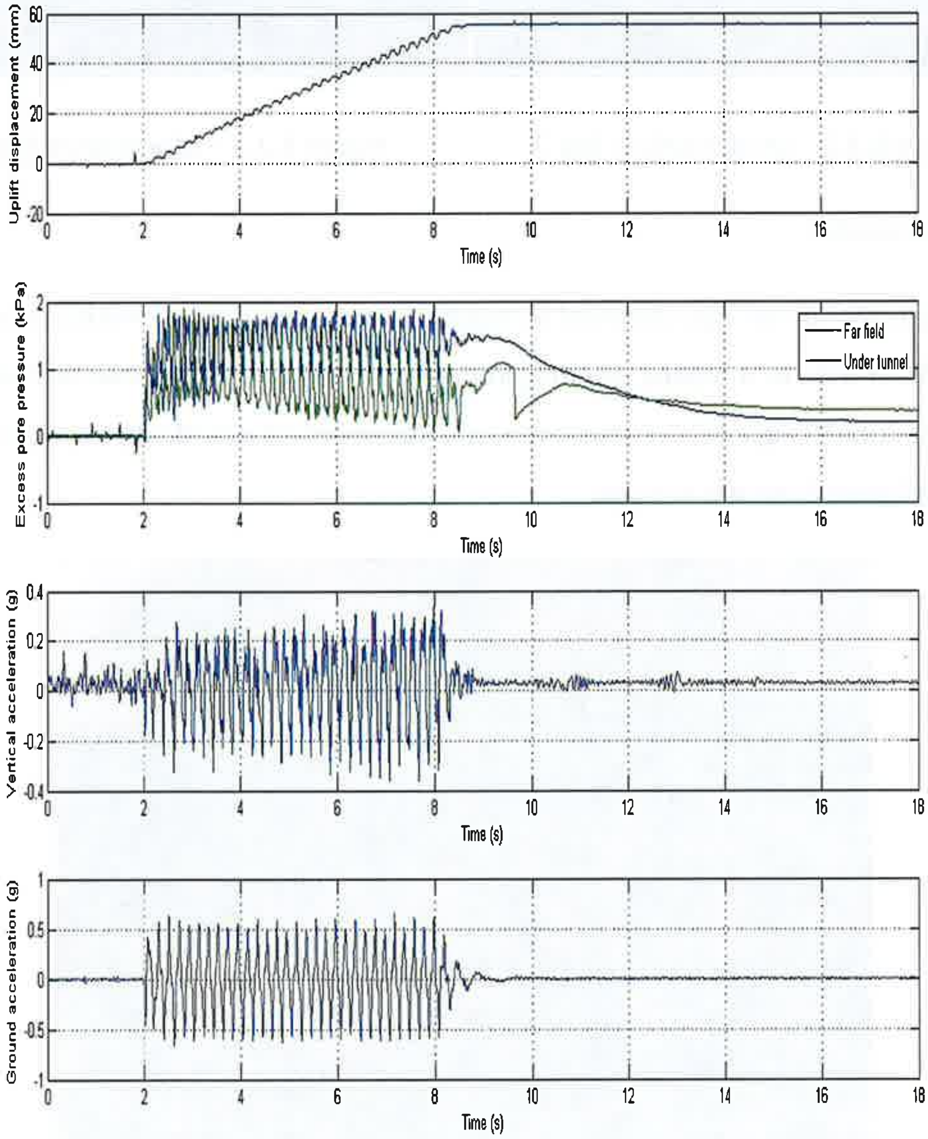

Figure 5.2.1 - Plots of uplift displacement, excess pore pressure, vertical acceleration and ground acceleration for Test 2

Figures 5.2.2 and 5.2.3 show the model before and after the experiment.

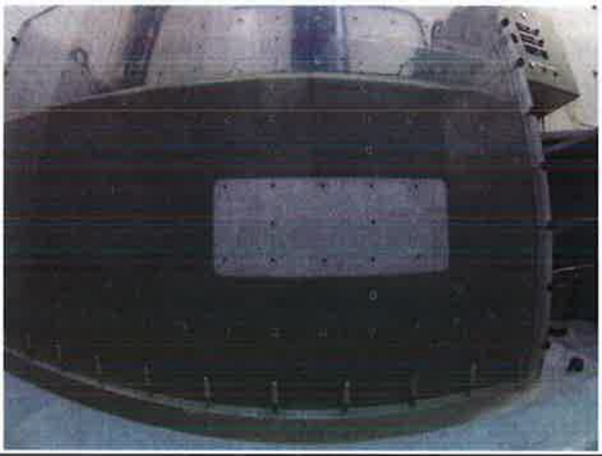

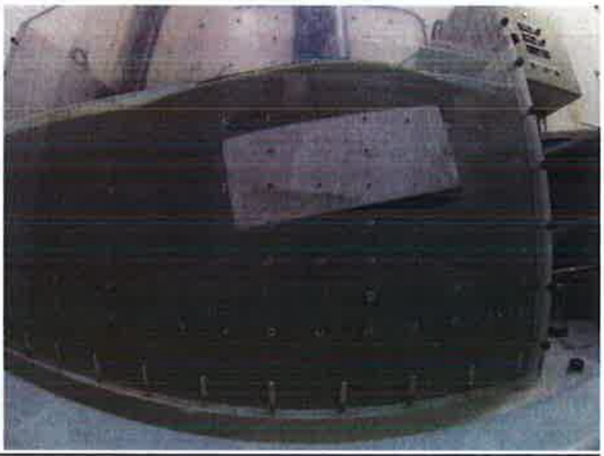

Figure 5.2.2 – Model before Test 2

Figure 5.2.3 – Model after Test 3

5.2.2 – Observations

As with Test 1, the tunnel was observed to move upwards with sudden motions during the shaking and to rotate as it moved resulting in the formation of a void below the bottom right corner of the tunnel. Figure 5.2.4 shows the soil movement observed when analysing the recorded high speed camera footage.

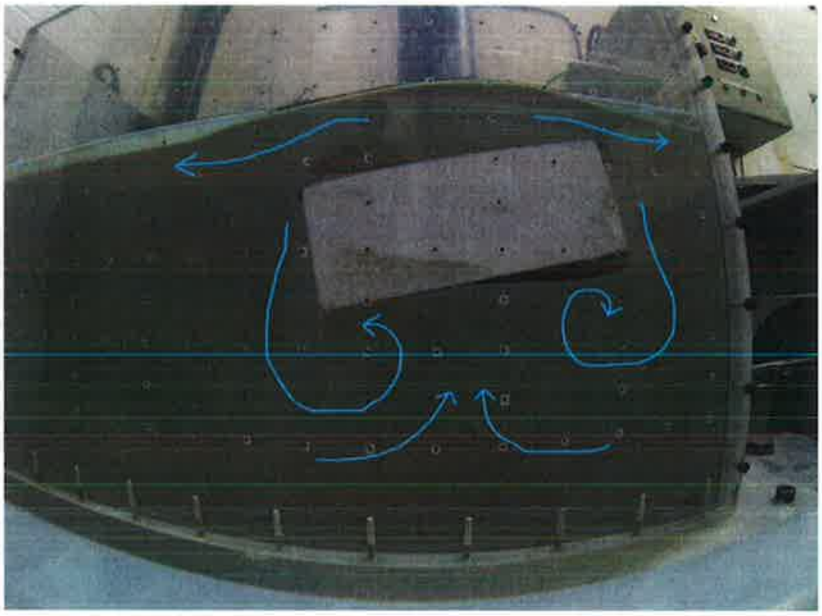

Figure 5.2.4 – Diagram of observed soil movement during Test 2

Again, there is a degree of "swirling" and turbulence to the soil motion immediately below the bottom corners of the tunnel, in this case to a greater extent than that observed during Test 1.

5.2.3 - Pore pressures

The second graph in Figure 5.2.1 shows that an average excess pore pressure of 1.36 kPa is generated in the far-field during shaking with the excess pore pressure after the shaking ceases but before dissipation of the excess pore pressures occurs of 1.474 kPa. The average excess pore pressure beneath the tunnel during shaking is 0.93 kPa and the excess pore pressure after the shaking but before dissipation is 1.0924 kPa. The peak amplitude of the oscillation of the excess pore pressure is 0.453 kPa in the far-field and 0.667 kPa underneath the tunnel. No negative pore pressures occurred during the earthquake.

The calculated value of excess pore pressure which would cause tunnel floatation to occur at a burial depth of 100mm is 0.49 kPa. The calculated value of excess pore pressure which causes full liquefaction of the sand at this depth is 0.869 kPa. The recorded excess pore pressures during this test for both the far field and underneath the tunnel exceed both of these values during their oscillations, showing that full liquefaction will have occurred during this experiment. As with Test 1, the excess pore pressures are high enough to occasionally generate negative effective stress. As full liquefaction is observed, significant uplift displacements would be expected. The post-earthquake image in Figure 5.2.3 clearly shows that significant uplift displacement did occur, with large distortions of the sand surface occurring.

5.2.4 - Vertical acceleration

The vertical accelerations during Test 2 are of a similar magnitude to those recorded in Test 1, with a peak value of around 0.3g and peak-to-peak vertical accelerations of around 0.6g. In this test, there is a slight increase in the magnitude of the vertical acceleration as the earthquake progresses. This suggests that as the tunnel floats upwards and the volume of sand above the tunnel decreases, the resultant buoyancy force driving the upward displacement of the tunnel and causing it to accelerate vertically increases. As with Test 1, the vertical acceleration of the tunnel corresponds well with the jerky vertical movement of the tunnel during the earthquake.

5.2.5 - Uplift displacement

As the excess pore pressures are high enough to cause full liquefaction underneath the tunnel, a significant uplift displacement would be expected. Comparison of the two images in Figures 5.2.2 and 5.2.3 show that this displacement does take place with large deformations of the sand surface taking place. The uplift displacement recorded using the draw wire for this test was 55.45mm, which is very similar to the amount of uplift displacement observed in Test 1.

5.3 - Test 3 – burial depth : 200mm

5.3.1 - Results

Figure 5.3.1 below shows the graphs of uplift displacement, excess pore pressure generated, vertical acceleration and ground acceleration for the third test, which was carried out at a burial depth of 200mm.

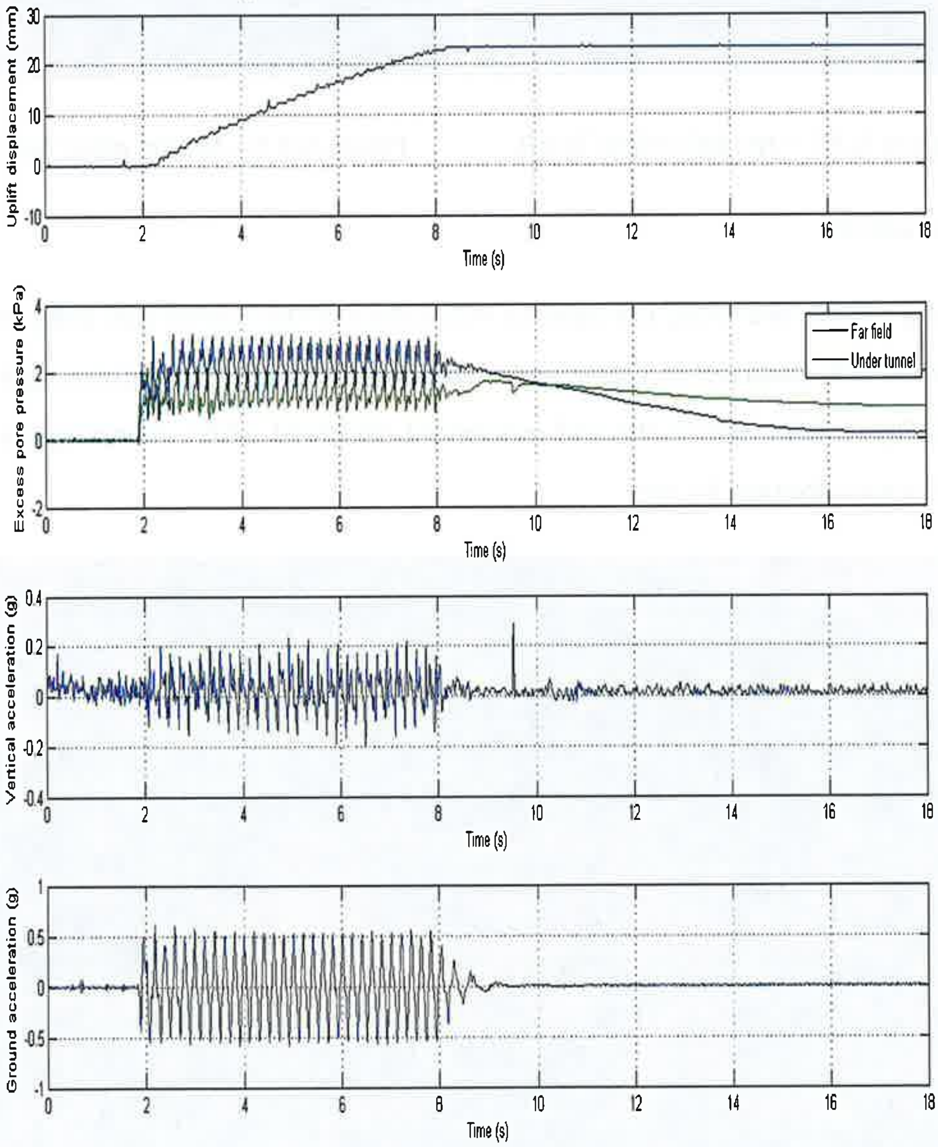

Figure 5.3.1 - Plots of uplift displacement, excess pore pressure, vertical acceleration and ground acceleration for Test 3

Figures 5.3.2 and 5.3.3 show the model before and after the experiment.

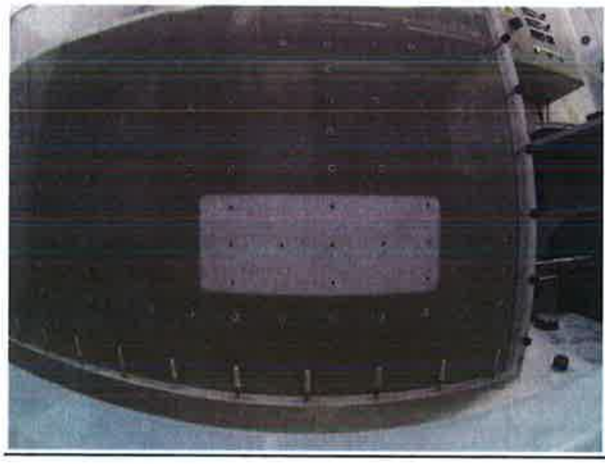
Figure 5.3.2 – Model before Test 3

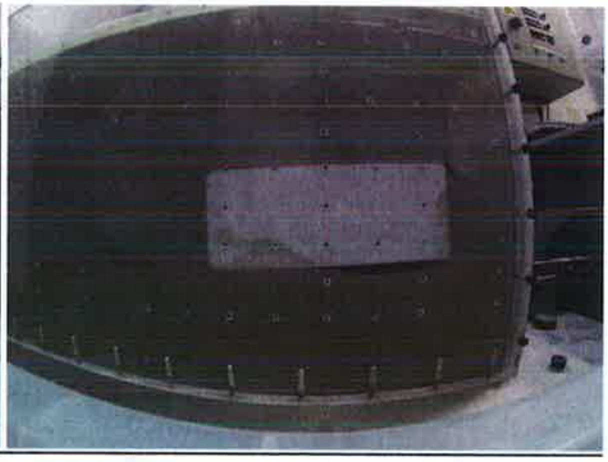
Figure 5.3.3 – Model after Test 3

5.3.2– Observations

As with the previous two tests, the upward movement of the tunnel was jerky and sudden and the tunnel was observed to rotate and a void formed below the bottom right corner of the tunnel. Figure 5.3.4 shows the soil movement observed when analysing the recorded high speed camera footage by eye.

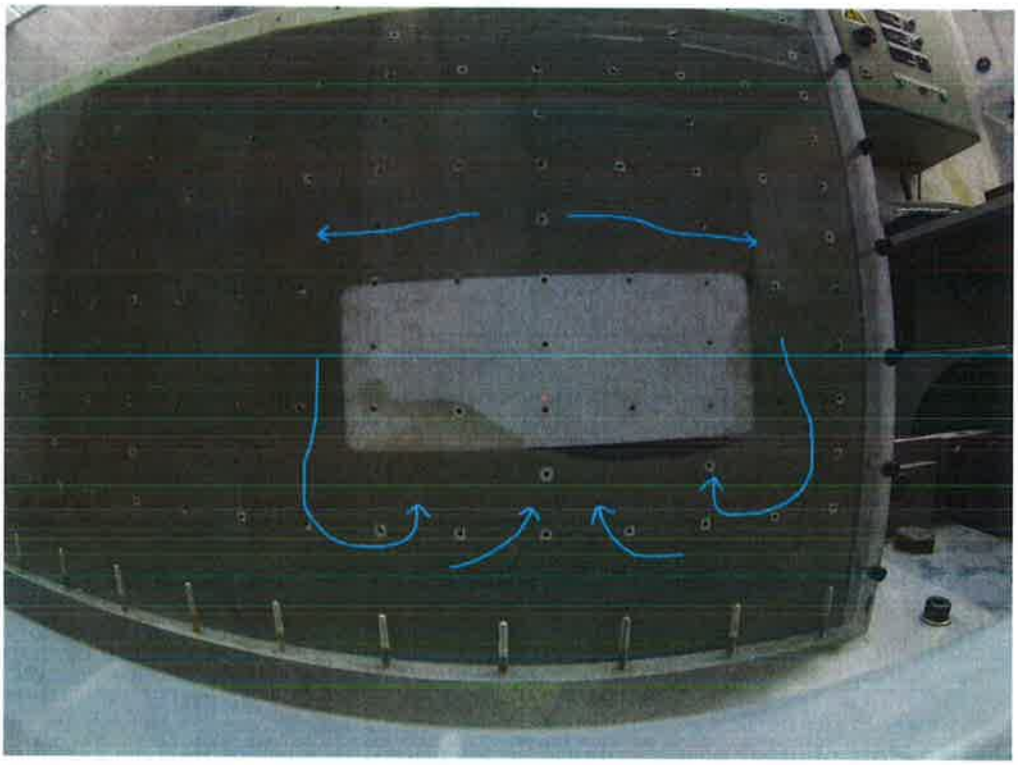
Figure 5.3.4 – Diagram of observed soil movement during Test 3

As before, the soil motion was somewhat turbulent below the bottom corners of the tunnel, although in this test this occurred to a much lesser extent than in the previous two experiments.

5.3.3 - Excess pore pressures

The graph of excess pore pressures in Figure 5.3.1 shows that the average excess pore pressure generated in the far-field during the shaking test was 2.51kPa with the excess pore pressure after shaking has stopped but before dissipation of the excess pore pressures occurs being 2.121 kPa. The average excess pore pressure generated underneath the tunnel during shaking is 1.45 kPa and the excess pore pressure when shaking has ceased and before dissipation of the excess pore pressure occurs is 1.687 kPa. The peak-to-peak amplitude of the excess pore pressure oscillation during the earthquake is 1.658 kPa in the far-field and 0.928 kPa beneath the tunnel.

The calculated value of excess pore pressure required for tunnel floatation to occur at a burial depth of 200mm is 1.36 kPa and the excess pore pressure required for full liquefaction to occur is 1.738 kPa. The recorded excess pore pressures in the far-field suggest that full liquefaction will definitely occur. However, the recorded excess pore pressures underneath the tunnel suggest that full liquefaction will only just occur and will in fact not take place during most of the earthquake. As full liquefaction does not take place during most of the earthquake, a less significant displacement than those which occurred in Tests 1 and 2 would be expected, despite the higher excess pore pressures being generated.

5.3.4 - Vertical accelerations

The recorded vertical accelerations during this test are of a very similar amplitude to the vertical accelerations recorded in Tests 1 and 2, with a peak positive acceleration of around 0.2g and a peak-to-peak acceleration of 0.4g. The acceleration oscillations occur at the same frequency as the ground accelerations and correspond well with the jerky vertical movement of the tunnel recorded during the experiment. The noisy vertical acceleration after the shaking has ceased is likely to be caused by the tunnel settling slightly or continued slight vibrations of the soil as vibrations are still being reflected by the steel wall of the shaking table rig.

5.3.5 - Uplift displacement

As the excess pore pressures are not as high during this test when compared with the excess pore pressures required for floatation to occur and the excess pore pressure below the tunnel is only just above the value of excess pore pressure required for full liquefaction to occur and then only at its peak values, a less significant uplift displacement would be expected when compared with the uplift displacements which occur during Tests 1 and 2. This is confirmed by comparing the images of the tunnel before and after the earthquake which show a much smaller displacement of the tunnel and much less deformation of the sand surface. The actual recorded uplift displacement was 23.8mm, around half of the displacement recorded during tests 1 and 2.

6 - Comparison of tests

6.1 - Observations

All three tests show very similar tunnel and soil movement as observed during the experiment and recorded using the high speed camera. In all three experiments, the tunnel was observed to have some degree of rotation as it moved upwards and a large void formed underneath the lower right corner of the tunnel. The motion of the soil in all three experiments was very consistent, showing noticeable turbulence and "swirling" of the sand below the tunnel. This occurred to a lesser degree in the third test, most likely due to the lower uplift displacement of the tunnel during this experiment. Figure 6.1.1 shows the soil movement from the second experiment and Figure 6.1.2 shows the expected result using the hypothesis that the soil movement will resemble the flow of fluid around a rectangular prism.

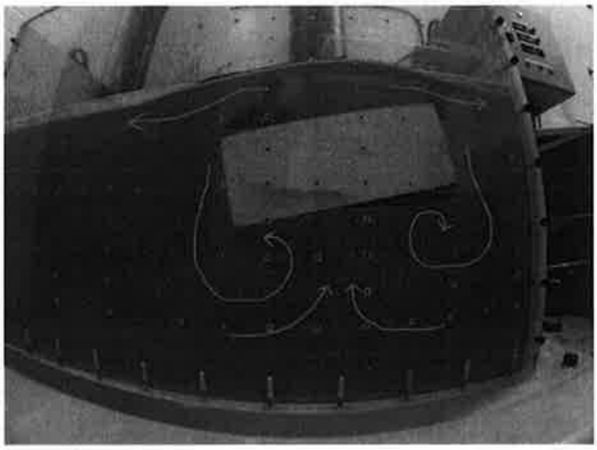

Figure 6.1.1 – Diagram of soil motion from Test 2

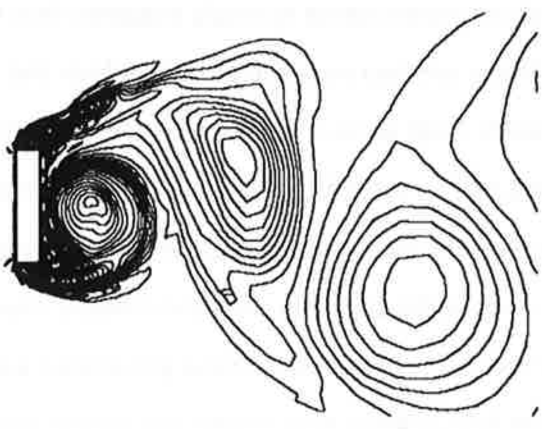

Figure 6.2.2 – Fluid flow past a rectangular cylinder (Matsukawa and Nakamura, 1987)

By comparing these two images, it is clear that this hypothesis was correct and the flow of soil around a rectangular tunnel as it floats upward during an earthquake does closely resemble the fluid flow around a rectangular prism.

6.2 - Pore pressures

Figure 6.2.1 shows the recorded excess pore pressures for Test 2 as a typical example of the excess pore pressures recorded in each of the three experiments conducted.

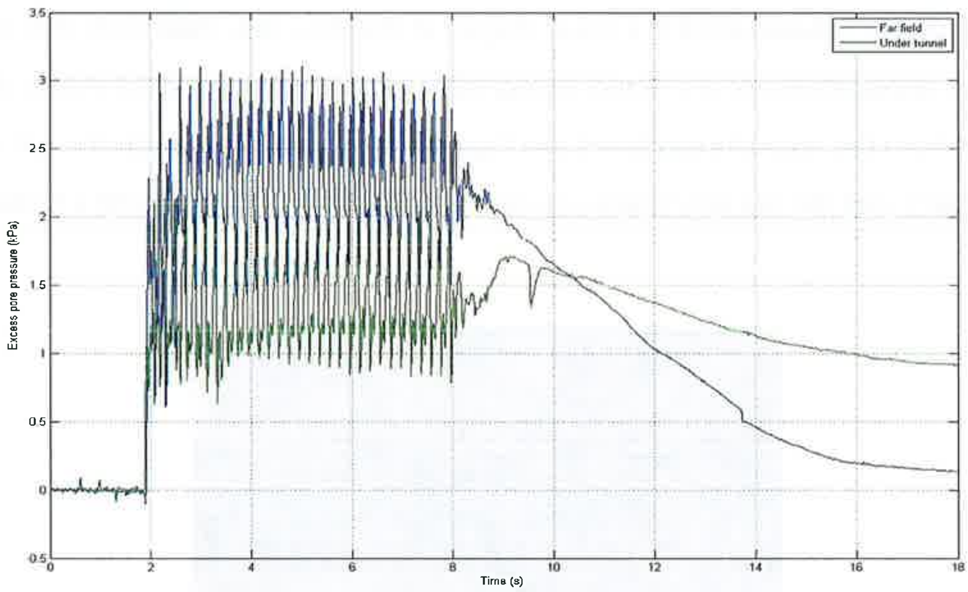

Figure 6.2.1 – Typical excess pore pressures, taken from Test 2

For all three experiments, the far field excess pore pressures generated during the shaking of the model were higher than the excess pore pressures recorded beneath the tunnel. The fact that this occurred in all three experiments strongly suggests that this difference is caused by the tunnel itself. There are two possible ways in which the tunnel could cause the excess pore pressure underneath itself to be lower than in the far field. The tunnel is less dense than the saturated sand and so the effective stresses below the tunnel are lowered, which could have an influence on the excess pore pressures generated. Alternatively, the motion of the tunnel in the sand, particularly the vertical motion, could cause the excess pore pressures below the tunnel to be lower than those generated away from the tunnel. It is also possible that the tunnel being closer to the side wall of the shaking table rig than originally intended may have had some influence on the excess pore pressures generated underneath the tunnel due to the vibrations reflecting off the steel wall.

In both the far field and underneath the tunnel, the excess pore pressure generated during the shaking increases with burial depth. However, because the excess pore pressure required to cause floatation and the pore pressure required to induce full liquefaction of the soil also increases with burial depth and does so at a faster rate than that at which the excess pore pressure increases with depth, the degree of liquefaction and hence the amount of floatation which occurs during the earthquake decreases with increased burial depth.

During the earthquakes, the far field excess pore pressures and those generated beneath the tunnel oscillated with similar amplitudes to each other and at approximately the same frequency as the ground motions. By comparing the oscillations of the excess pore pressure with the ground acceleration trace, it becomes apparent that a positive ground acceleration causes increased excess pore pressure and when the ground accelerations are negative, this causes the excess pore pressure to decrease and can even cause the excess pore pressure to become negative, resulting in a slight and very brief increase in the strength and stiffness of the soil.

6.3 - Vertical accelerations

Figure 6.3.1 shows the vertical accelerations recorded during all three of the experiments.

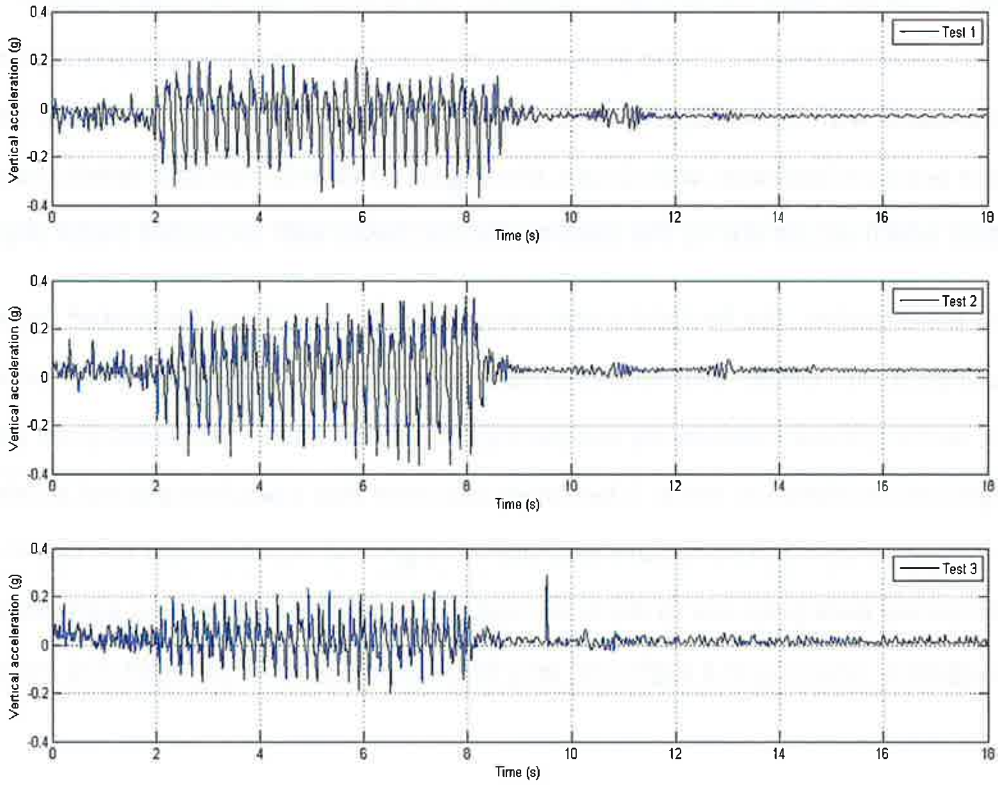

Figure 6.3.1 – Vertical accelerations during all three experiments

All three tests show very similar vertical accelerations with only slight differences between the vertical accelerations of the tunnel during Tests 1 and 3 and an increasing vertical acceleration during Test 2. The similarity between the vertical accelerations during Tests 1 and 3 suggests that the vertical acceleration of the tunnel during floatation depends very little on the burial depth of the tunnel. It is likely that the ground acceleration is the main factor which determines the vertical accelerations of the tunnel during an earthquake. However, as earthquakes of differing ground accelerations were not examined during this project, it is difficult to say with absolute certainty that the ground acceleration is indeed the main factor which determines the vertical acceleration of a tunnel during floatation.

Although increased burial depth appears to have little effect on the vertical acceleration of the tunnel during floatation, an increase in the vertical acceleration of the tunnel of around

0.1g was recorded during test 2. This is possibly because the weight of sand above the tunnel decreases as the tunnel floats upwards and the sand above the tunnel flows away, which causes the resultant uplift force acting on the tunnel to increase and hence the vertical acceleration of the tunnel increases. This slight increase would not be observed during either the first or third tests because during Test 1 very little of the sand above the tunnel actually flowed away and during Test 3 the uplift of the tunnel did not cause much soil movement or deformation of the sand surface compared with the movements and deformations observed during Tests 1 and 2.

6.4 - Uplift displacement

Figure 6.4.1 shows the recorded uplift displacements of the tunnel during the three experiments.

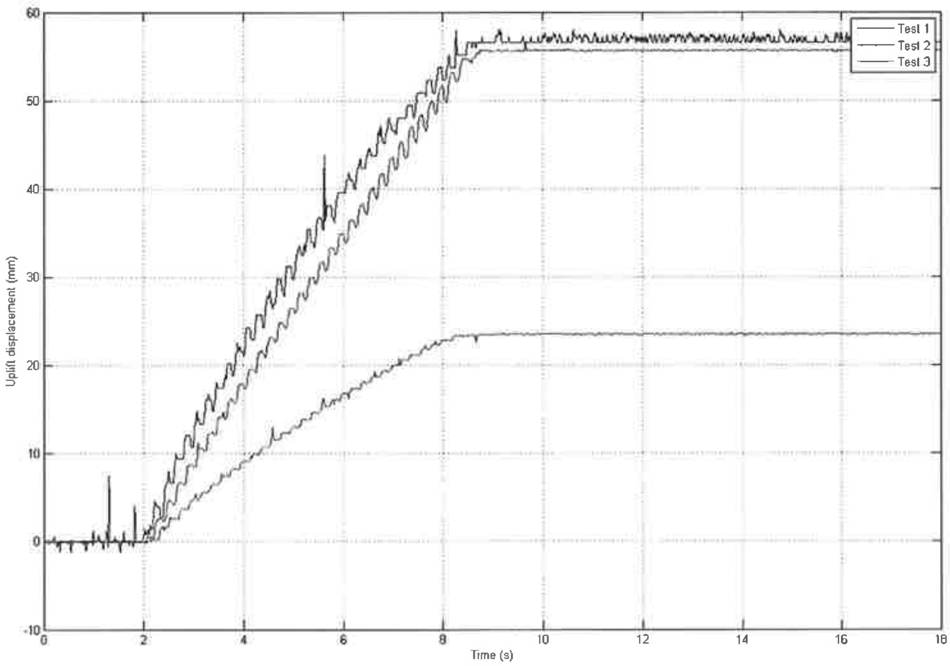

Figure 6.4.1 – Uplift displacements during all three experiments

The uplift displacements recorded during the first and second tests are almost exactly the same as each other. The obvious explanation for this is that in Test 1 the tunnel was displaced upwards by a distance greater than its original burial depth, causing the tunnel to break through the surface of the sand. Once the tunnel has broken the surface of the sand, the pressure difference between the top of the tunnel and the bottom of the tunnel decreases and the tunnel eventually becomes no longer able to move upwards. This limitation on displacement doesn't apply to the tunnel during Test 2 and so the uplift displacements of the tunnel during Tests 1 and 2 can quite easily be the same.

The uplift displacement of the tunnel recorded in Test 3 is 23.8mm, around half of the displacement recorded during Test 2. As the burial depth of the tunnel during Test 3 was twice the burial depth of the tunnel during Test 2, this suggests that the uplift displacement of a tunnel during floatation is inversely proportional to the burial depth of the tunnel. However, further tests would be needed at different depths to confirm this.

7 - Conclusions

Through the experiments conducted during this project, the following conclusions have been reached:

- The excess pore pressure required to cause floatation and to induce full liquefaction of the soil both increase with increasing depth. As such, although the excess pore pressure generated during an earthquake appears to increase with depth, the degree of liquefaction which occurs decreases with increasing depth as the required excess pore pressure to cause full liquefaction increases by a greater amount with increased depth than the excess pore pressure generated does.
- The recorded uplift displacement of the tunnel during the experiment clearly decreases with depth. By comparing the uplift displacements recorded during Tests 2 and 3, it appears that the uplift displacement of a tunnel during floatation is inversely proportional to the burial depth of the tunnel.
- By comparing the observed motion of the tunnel with an image of the fluid flow around a rectangular prism, it becomes clear that the two images closely resemble one another. As such, it can be concluded that the flow of soil around a rectangular tunnel during floatation of the tunnel is very similar to the flow of fluid around a rectangular prism.

8 - Future Work

It was originally intended that PIV analysis would be carried out on the high speed camera footage of the experiments to more accurately determine the motion of the tunnel and soil during floatation of the tunnel. However, time constraints meant that this was not possible. As such, an obvious area for future work would be to carry out PIV analysis on recorded high speed footage of a rectangular tunnel undergoing floatation in liquefied soil to more accurately determine the motion of the tunnel and the soil.

Other areas in which future work could be carried out include:

- Repeating the experiments using tunnels of different aspect ratios.
- Repeating the experiments using smaller tunnels of the same aspect ratio as the tunnel used in these experiments to enable a wider range of burial depth to diameter ratios to be examined.
- Repeating the experiments with earthquakes of different ground accelerations.
- Determining the floatation mechanism of tunnels of other shapes such as elliptical tunnels.

Appendix A – Calculations of factors of safety against floatation and required excess pore pressures to cause floatation and full liquefaction

Figure A.1 shows the minimum and maximum voids ratios for Hostun sand and the specific gravity of Hostun sand. Figure A.2 lists the dimensions and mass of the tunnel used in this project.

Maximum voids ratio, e_{max}	Minimum voids ratio, e_{min}	Specific gravity, G_s
1.067	0.555	2.65

Figure A.1 – Hostun sand data

Length, l (mm)	Width, b (mm)	Depth, h (mm)	Mass (kg)
300	200	80	2.5

Figure A.2 – Tunnel dimensions and mass

Using the pouring method outlined in section 4.1, a typical loose relative density, I_D, that can be reached is around 0.4. Assuming this relative density, the voids ratio of the sand will be:

$$e = e_{max} - I_D(e_{max} - e_{min}) = 1.067 - 0.4(1.067 - 0.555) = 0.8622$$

The buoyant unit weight of the sand when it is fully saturated and with this voids ratio will be:

$$\gamma' = \left(\frac{G_s - 1}{1 + e}\right)\gamma_w = \left(\frac{2.65 - 1}{1 + 0.8622}\right)9.81 = 8.7kN/m^3$$

The buoyant weight of the sand above the tunnel, and hence the force acting on the tunnel due to the sand will be:

$$F_{SAND} = \gamma' dbl = 8700 \times 0.2 \times 0.3 \times d = 26.1N \; when \; d = 50mm$$

$$F_{SAND} = 52.2 \; N \; when \; d = 100mm$$

$$F_{SAND} = 104.4 \; N \; when \; d = 200mm$$

where d is the burial depth of the tunnel.

The self weight of the tunnel, $F_{SELF-WEIGHT}$, is 24.5N.

The buoyancy force due to hydrostatic pressure differences is:

$$F_{BUOYANCY} = \rho_w ghbl = 1000 \times 9.81 \times 0.08 \times 0.2 \times 0.3 = 47.1N$$

The factor of safety against floatation is calculated as:

$$FoS\ against\ floatation = \frac{F_{SAND} + F_{SELF-WEIGHT}}{F_{BUOYANCY}}$$

$$FoS\ against\ floatation = 1.07\ when\ d = 50mm, 1.63\ when\ d = 100mm, 2.74\ when\ d = 200mm$$

At the point of floatation –when the factor of safety against floatation is equal to 1 – the buoyant weight of the sand above the tunnel is 22.6N.

The buoyant weight of the sand can be calculated in terms of the pore pressure in the soil and the saturated unit weight of the sand as:

$$F_{SAND} = \gamma dbl - ubl$$

As such, the required excess pore pressure to induce floatation can be calculated as:

$$u_{excess} = \frac{F_{SAND} - 22.6}{bl} = 0.06kPa\ when\ d = 50mm, = 0.49kPa\ when\ d = 100mm, = 1.36kPa\ when\ d = 200mm.$$

Full liquefaction of soil occurs at the point where the effective stress, σ', is equal to zero. As such, the required excess pore pressure to induce full liquefaction of the soil can be calculated as:

$$u_{excess} = \gamma' d = 0.435kPa\ when\ d = 50mm, = 0.869kPa\ when\ d = 100mm, = 1.738kPa\ when\ d = 200mm$$

Appendix B – Risk assessment

The initial risk assessment was carried out with the assistance of Prof. Gopal Madabhushi. The hazards which were recognised at this stage included heavy lifting of sand, water and equipment; sand pouring and associated risks of inhalation of fine sand particulates; and working with liquids and electrical equipment. The steps taken to mitigate these risks included using lifting equipment when moving heavy or bulky objects to minimise risk of injury and the use of extractors and respirator masks when pouring sand to mitigate the risk of inhalation of fine sand particulates.

One hazard which came up during the course of the project that was not identified in the initial risk assessment was the use of metallic ink to dye some of the sand. The steps taken to mitigate the risks associated with this include using disposable gloves when handling the ink to prevent skin contact with it and ensuring that the working area was as well ventilated as possible to mitigate the risks associated with the ink fumes.

References

Cameron, I., (2013). *Visualisation of Shallow Foundation Failure following Earthquake Induced Liquefaction*. M.Eng. University of Cambridge.

Chian, S.C., (2012). *Floatation of Underground Structures in Liquefiable Soils*. Ph.D. University of Cambridge.

Ishihara, K., (1993), *Thirty Third Rankine Lecture: Liquefaction and flow failure during earthquakes* Géotechnique Volume 43, pp 349-417.

Yasuharu Nakamura and Tohru Matsukawa (1987). *Vortex excitation of rectangular cylinders with a long side normal to the flow.* Journal of Fluid Mechanics, 180, pp 171-191 doi:10.1017/S0022112087001770

Acknowledgements

Many thanks go to Professor Gopal Madabhushi, Dr Stuart Haigh and Charlie Heron for offering considerable guidance and assistance throughout this project.